# Dissecting in vivo steady-state dynamics of karyopherin-dependent nuclear transport

Ogheneochukome Lolodi[a], Hiroya Yamazaki[a], Shotaro Otsuka[b], Masahiro Kumeta[a], and Shige H. Yoshimura[a]

[a]Graduate School of Biostudies, Kyoto University, Kyoto 606-8501, Japan; [b]European Molecular Biology Laboratory, 69117 Heidelberg, Germany

**ABSTRACT** **Karyopherin-dependent molecular transport through the nuclear pore complex is maintained by constant recycling pathways of karyopherins coupled with the Ran-dependent cargo catch-and-release mechanism. Although many studies have revealed the bidirectional dynamics of karyopherins, the entire kinetics of the steady-state dynamics of karyopherin and cargo is still not fully understood. In this study, we used fluorescence recovery after photobleaching and fluorescence loss in photobleaching on live cells to provide convincing in vivo proof that karyopherin-mediated nucleocytoplasmic transport of cargoes is bidirectional. Continuous photobleaching of the cytoplasm of live cells expressing NLS cargoes led to progressive decrease of nuclear fluorescence signals. In addition, experimentally obtained kinetic parameters of karyopherin complexes were used to establish a kinetic model to explain the entire cargo import and export transport cycles facilitated by importin β. The results strongly indicate that constant shuttling of karyopherins, either free or bound to cargo, ensures proper balancing of nucleocytoplasmic distribution of cargoes and establishes effective regulation of cargo dynamics by RanGTP.**

**Monitoring Editor**
Karsten Weis
ETH Zurich

Received: Aug 28, 2015
Revised: Oct 22, 2015
Accepted: Oct 27, 2015

## INTRODUCTION

Macromolecular transport across the nuclear envelope is tightly regulated by nuclear pore complexes (NPCs), which are large protein complexes embedded in the envelope (Ohno *et al.*, 1998; Fahrenkrog *et al.*, 2001; Rout and Aitchison, 2001; Vasu and Forbes, 2001). The central channel of each NPC is filled with its subunits (nucleoporins [Nups]), which are rich in hydrophobic amino acids, and thus it functions as a hydrophobic size-selective barrier (Ribbeck and Gorlich, 2002; Wente and Rout, 2010). These features, as well as the crowded environment of the NPCs, prevent an unregulated, free exchange of macromolecules between the cytoplasm and the nucleoplasm (Timney *et al.*, 2006; Yang and Musser, 2006; Tetenbaum-Novatt *et al.*, 2012). Small and hydrophobic molecules, with a maximum size in the range of 20–40 kDa, are able to pass through the NPC by passive diffusion, but large and hydrophilic molecules cannot; their passage usually requires transport mediators (Paine *et al.*, 1975; Gorlich and Kutay, 1999; Pante and Kann, 2002; Peters, 2009).

Karyopherins, which are arguably the most widely studied nuclear transport mediators, facilitate the transport of a vast array of cellular proteins/molecules (Cingolani *et al.*, 1999, 2002; Strom and Weis, 2001; Lee *et al.*, 2003; Cansizoghu *et al.*, 2007). In spite of their large molecular sizes (~100 kDa), karyopherins can pass through the nuclear pore by themselves and also together with their specific cargoes. This ability of karyopherins is mostly attributed to their unique structure, which is characterized by the presence of several repeats of the HEAT motif, which comprises a pair of amphiphilic α-helices. Karyopherins and other HEAT-rich proteins have been demonstrated to undergo flexible conformational changes that enable them to pass through the hydrophobic milieu of the pore (Kumeta *et al.*, 2012; Yoshimura *et al.*, 2014).

Although the HEAT repeat is suitable for overcoming the hydrophobic barrier, the question still remains whether karyopherins have intrinsic directionality through the pore (Chook and Blobel, 1999). During translocation across the NPC, karyopherins interact with a number of Nups, mainly via transient hydrophobic interactions (Rout *et al.*, 2000; Frey *et al.*, 2006; Frey and Gorlich, 2007; Lim *et al.*, 2006; Patel *et al.*, 2007; Hutten *et al.*, 2008). In vitro measurement of

This article was published online ahead of print in MBoC in Press (http://www.molbiolcell.org/cgi/doi/10.1091/mbc.E15-08-0601) on November 4, 2015.

Address correspondence to: S. H. Yoshimura (yoshimura@lif.kyoto-u.ac.jp).

Abbreviations used: FLIP, fluorescence loss in photobleaching; FRAP, fluorescence recovery after photobleaching; NLS, nuclear localization signal; NPC, nuclear pore complex; Nup, nucleoporin; SPR, surface plasmon resonance.

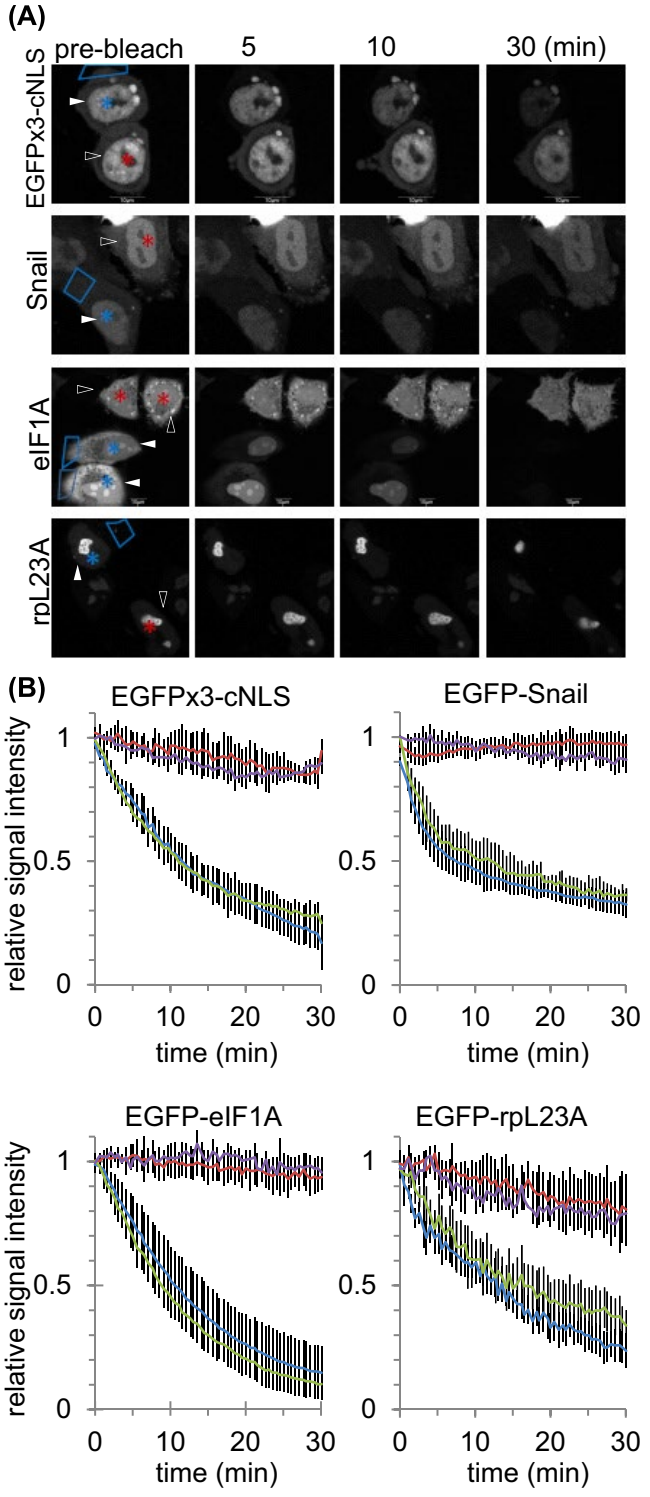


FIGURE 1: Influx and efflux dynamics of import cargoes in live cells. (A) FLIP analysis of EGFP-labeled cargoes in HeLa cells. Three tandem EGFPs fused with a cNLS (EGFPx3-cNLS), EGFP-tagged Snail, eIF1A, and rpL23A were expressed in HeLa cells. Portions of the cytoplasm (indicated by the blue regions) of cells (closed arrowheads) were subjected to continuous bleaching for 30 min. The signal intensities in the corresponding nuclei (blue asterisks) and the control nuclei (red asterisks) were measured. (B) Quantification of nuclear signal intensities in A and in the presence of 5 ng/ml leptomycin B (LMB; Supplemental Figure S1C). Relative signal intensity of bleached and nonbleached nuclei are plotted (blue and red for bleached and nonbleached, respectively), together with LMB-treated results (green and purple for bleached and nonbleached, respectively). The same measurements were performed in a minimum of 10 different cells for averaging. The error bars represent SDs. A monoexponential decay curve, $Y = a \exp(k_{out}X) + c$, was fitted to the data, and the kinetic constant, $k_{out}$ was obtained from the mobile fraction. The immobile fraction, $c$, for EGFPx3-cNLS, EGFP-eIF1A, EGFP-rpL23A, and EGFP-Snail was estimated to be 11, 18, 34, and 35%, respectively. The Student's $t$ test confirmed that LMB treatment did not cause a statistically significant difference between the $k_{out}$ values (Supplemental Figure S2A).

importin β-Nup interaction revealed that Nups might have different affinity for importin β (Ben-Efraim and Gerace, 2001), suggesting that importin β might move toward the nucleoplasm, depending on the increasing affinity with Nups (affinity gradient; Shah and Forbes, 1998; Ribbeck and Gorlich, 2001). Consequently, an intrinsic directionality of importin β was reasonably propounded to explain the directional inward transport of the cargo. However, this model was redefined after observations that it is limited by the requirement of other protein(s) or mechanism(s) to release importin β from the NPC and recycle it back to the cytoplasm (Zilman *et al.*, 2007). In addition, structural differences between importins and exportins that could explain opposite directionality have not been reported.

Nondirectional models, on the other hand, do not require any other proteins for karyopherins to shuttle across the NPC and also can explain the active transport of cargo when combined with RanGTP-dependent cargo-catch/release mechanism (Gorlich *et al.*, 1996, 2003). It has been shown that in in vitro transport assay systems, importin β can pass through the NPC in both directions (bidirectional; Gorlich and Kutay, 1999). For such bidirectional passage of karyopherins to establish a cargo gradient across the NPC, the entire transport system requires a number of interaction kinetics involving karyopherins, RanGTP, and the cargo, as well as the appropriate concentration of each component in living cell compartments. Although in vitro transport assay demonstrates that this model can establish the cargo gradient, it is not clear whether this works in living cells.

In this study, we performed quantitative analyses of karyopherin-dependent cargo transport in vivo to elucidate how the karyopherin–cargo complex shuttles through the NPC and maintains the cargo gradient across the nuclear envelope. We integrated flux rate constants obtained from in vitro transport assay and the binding–unbinding rate constants of karyopherin–cargo interaction with dynamic measurements of fluorescently labeled cargoes and karyopherins in live cells, using fluorescence recovery after photobleaching (FRAP) and fluorescence loss in photobleaching (FLIP) assays. These analyses elucidate the intracellular dynamics of each transport component and how they are integrated into the entire transport system to reach to a certain equilibrium state in a cell.

## RESULTS

### Steady-state shuttling of import cargo across the nuclear envelope in a living cell

There is evidence that HeLa cells endogenously express almost all of the known karyopherins in physiologically relevant amounts (Yaseen and Blobel, 1997; Mingot *et al.*, 2001; Miyamoto *et al.*, 2004; Van der Watt *et al.*, 2009). Therefore, in the in vivo aspect of this study, we monitored well-established cargoes of some of the karyopherins. Enhanced green fluorescent protein (EGFP)–Snail (a cargo for importin β1) was expressed in HeLa cells and analyzed by FLIP with continuous bleaching of the cytoplasm. As shown in Figure 1A, the

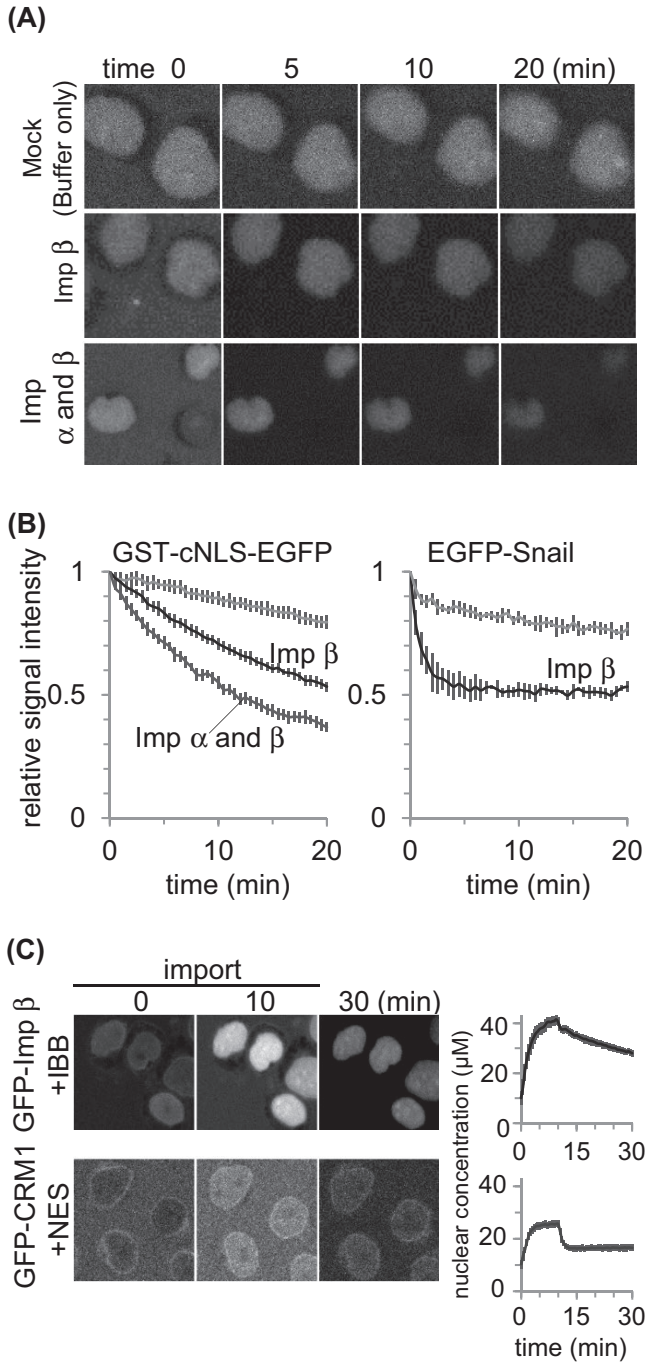


FIGURE 2: Ran-independent export of import cargoes by importin β. (A) Semipermeabilized cells were preloaded with fluorescently labeled cargo (GST-cNLS-EGFP) by incubation in the presence of importin α and β, RanGDP, and an ATP regeneration system for 10 min. Afterward, the external medium was replaced with only buffer (top), buffer containing importin β (middle), or buffer with both importin α and β (bottom). Time-lapse microscope observation was performed for 20 min. Captured images at times 0, 5, 10, and 20 min are shown. (B) Signal intensity within each nucleus in A was quantified, averaged, and plotted against time; HeLa nuclei preloaded with GFP-cNLS-EGFP (left) and EGFP-Snail (right). The same measurements were performed in a minimum of five different cells. The error bars represent SDs. (C) Top, 4 μM each of GFP-fused importin β, RanGDP, and IBB, as well as an ATP regeneration system, was added to the external medium of digitonin-treated HeLa cells. Bottom, 1 μM GFP-fused CRM1, 4 μM RanGDP, and 1 μM NES peptide were also added to semipermeabilized cells. The observation was performed for 10 min, and then the external medium was replaced with the buffer without any protein, and observation was continued for another 20 min. The average fluorescence intensity of the nucleoplasm was measured, converted to concentration, and plotted against time (right). The same measurements were performed in a minimum of five different cells. The error bars represent SDs.

nuclear signal of the cargo was significantly reduced compared with the nonbleached control cells in the same image (sample size $n = 10$ for both FLIP and control analyses). Similar results were obtained for the cargoes of other importin β family proteins (rpL23A for importin 5 and eIF1A for importin 13), as well as for three tandem EGFPs fused with a classical nuclear localization signal (cNLS) of SV40 large T-antigen (EGFPx3-cNLS) and cNLS-EGFP-eIF4A1, which are imported by the importin α/β pathway (Figure 1A and Supplemental Figure S1, A and B). These results indicate that import cargoes always shuttle between the cytoplasm and nucleoplasm and do not stay sequestered in the nucleoplasm after their import by the importin-dependent pathway.

We then examined the effect of leptomycin B (LMB), a specific inhibitor of CRM1, on the efflux of the import cargo. Previous reports established that 5 ng/ml LMB for 4–24 h is sufficient to significantly block CRM1-dependent export pathway (Kudo *et al.*, 1998; Jang *et al.*, 2003; Kumeta *et al.*, 2010). Treatment of the cells with 5 ng/ml LMB for 5–8 h before FLIP analysis did not appreciably halt the egress of all import cargoes tested ($n = 10$; Figure 1B and Supplemental Figures S1C and S2A), suggesting that the nuclear export of the import cargo was not mediated by an export mediator such as CRM1.

### Shuttling of import cargo is mediated by importin

We then examined the involvement of importin β in the export of the import cargo. Digitonin-treated HeLa cells were preloaded with fluorescent import cargo (EGFP-Snail or glutathione *S*-transferase [GST]–cNLS-EGFP), and then the external medium was replaced with buffer alone or with buffer containing importin β. In the absence of importin β, the cargo signal in the nucleus did not diminish after 20 min ($n = 7$; Figure 2A, top), whereas incubation with importin β significantly reduced the nuclear cargo signal ($n = 6$; Figure 2, A, middle and bottom, and B). In the case of GST-cNLS-EGFP, the addition of importin α together with importin β accelerated the efflux of the cargo ($n = 4$; Figure 2B). The most plausible explanation is that free importin β from the external medium enters the nucleus, binds to the cargo, and then exits the nucleus in a complex with its cargo. Note that this importin β–dependent cargo efflux from the nucleus is Ran-independent.

Bidirectional passage of karyopherin–cargo complex is a common feature of both importins and exportins. Digitonin-treated HeLa cell nuclei were incubated either with importin β–cargo complex (importin β–binding domain of importin α [IBB] and GFP-importin β; Figure 2C, top), or exportin-cargo complex (nuclear export signal [NES] peptide and GFP-CRM1; Figure 2C, bottom). In both cases, the karyopherin–cargo complex swiftly entered the nuclei (10 min). Then the external medium was replaced with buffer without protein, and observation was continued for another 20 min. Both classes of karyopherin–cargo complex were able to leak out of the nuclei (30 min). These results indicate that karyopherin–cargo complex is able to shuttle across the NPC in both directions.

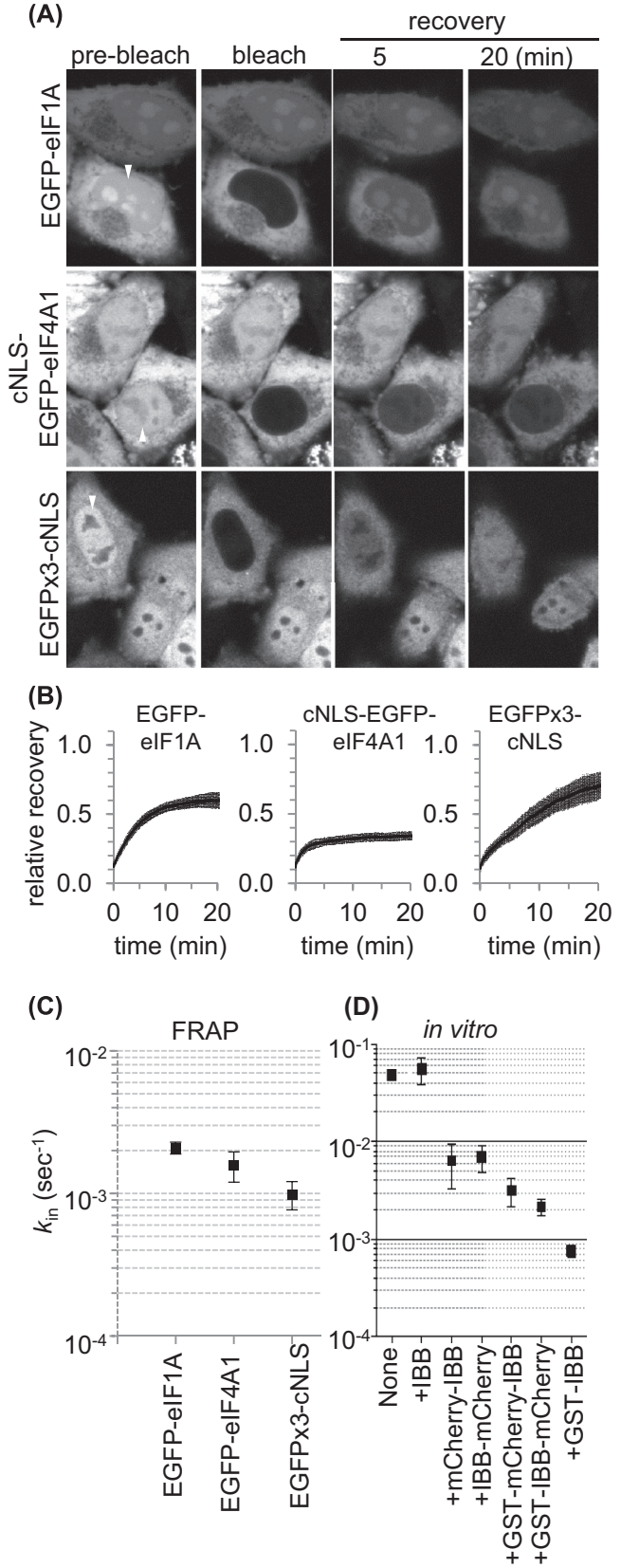


FIGURE 3: Cargo properties affect the flux rate of karyopherin–cargo complexes. (A–C) FRAP analysis of nuclear influx of different cargoes. (A) EGFP-labeled cargoes of importins ranging from ~50 to 100 kDa were transfected into HeLa cells for 24 h. Then the nucleus was bleached for 5 s and nuclear fluorescence recovery monitored every 3 s for 20 min. (B) Fluorescence recovery was quantified and presented as fluorescence intensity relative to prebleach intensity. The same measurements were performed in a minimum of five different cells. The error bars represent SDs. (C) An exponential curve was fitted to the FRAP data, and the indicated $k_{in}$ values were obtained. (D) The influx rate constants ($k_{in}$) of different-sized cargo proteins were determined by in vitro nuclear transport and summarized as shown. We added 4 μM each of EGFP-fused importin β, RanGDP, and indicated cargo, as well as an ATP regeneration system, to the external medium of digitonin-treated HeLa cells. Nuclear import was observed for 30 min and nuclear signal quantified thereafter. The data were fitted with a single exponential, and the kinetic constants, $k_{in}$ and $k_{out}$, were obtained. In general, the flux rate mostly depends on the size and/or hydrophobicity of the cargo. As the cargo size becomes larger, influx of importin β becomes slower.

### Cargo properties affect karyopherin–cargo flux

Next, we examined how the kinetics of importin β and cargo shuttling is affected by cargo properties. Cargoes of different sizes were expressed in HeLa cells, and their flux rates across the NPC were examined by FRAP analysis ($n$ = 5 for each cargo; Figure 3, A and B, and Supplemental Figure S3, A and B). There was an inverse relationship between the size and influx rate of EGFPx3-cNLS, cNLS-EGFP-eIF4A1, and EGFP-eIF1A, which have molecular weights of ~100, 73, and 50 kDa, respectively (Figure 3C). Passive permeability of these cargoes made negligible input to the observed flux rates, given that they did not show spontaneous passage through the NPC without the help of karyopherins (Supplemental Figure S3C).

Similar results were obtained in an in vitro assay in which IBB was fused with various proteins and preincubated with purified EGFP–importin β before being added to digitonin-treated HeLa cells. As summarized in Figure 3D, in general, the larger the cargo, the slower is its passage through the NPCs. The lower flux rates of GST-IBB in spite of its similar molecular weight to mCherry-IBB indicate that hydrophobicity of cargo might also affect transport rates.

### Building a kinetic model of the karyopherin-dependent cargo transport cycle

To dissect the foregoing experimental observations and quantitate the flux of each component (free importin, free cargo, importin–cargo complex, etc.), we developed a kinetic model of the karyopherin-dependent nuclear transport cycle, as shown in Figure 4. Two compartments—the nucleoplasm and cytoplasm—are delineated in the model, and karyopherins can travel between them with flux rate constants $k_{in}$ and $k_{out}$ for inward and outward directions, respectively. These fluxes occur for free importin β (Figure 4, step 6), importin β–cargo complex (step 5), and importin β–RanGTP complex (step 7; Figure 2C and Table 1). In addition to the fluxes, karyopherin, cargo, and Ran interact with each other in each compartment (steps 1 and 3), with association and dissociation rate constants $k_{on}$ and $k_{off}$, respectively. RanGTP-dependent dissociation of importin β from the cargo occurs in the nucleoplasm at an apparent rate constant of $k_{on}$[impβ-cargo-RanGTP] (step 2). For simplicity, RanGTP exists only in the nucleoplasm at a constant concentration due to the activity of chromatin-bound RCC1. Hydrolysis of RanGTP to RanGDP occurs in the cytoplasm because of the cytoplasmic localization of RanGAP (step 4). RanBP1 plays a critical role as a coactivator of RanGAP in this process due to its ability to form a RanGTP–RanBP1 complex, which serves as the optimal substrate for the enzymatic action of RanGAP (Bischoff and Gorlich, 1997; Kuhlmann *et al.*, 1997).

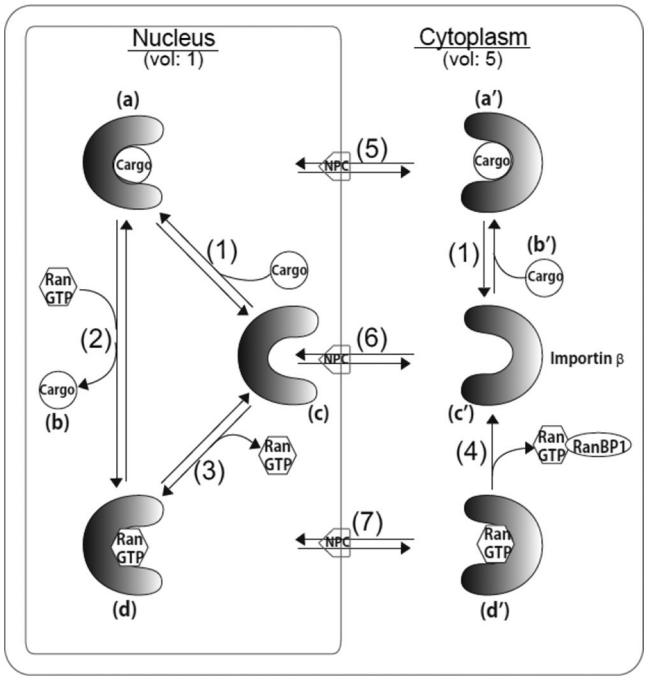


FIGURE 4: Kinetic model of importin β–dependent transport cycle. Rate constants (shown in Table 1 with corresponding numbers) from in vitro transport assay systems and SPR were used to design the model. Briefly, free importin β, importin β–cargo complex, and importin β–RanGTP complex pass through the NPC in both directions with the indicated flux rates. Details of the model and how the kinetic parameters (1–7) were obtained are described in the text (*Results*), Supplemental Figures S2B, S4, and S5, and Supplemental Experimental Procedure. The steady-state concentration of the components (letters in parenthesis shown in Table 2) were obtained by simulation of in vivo dynamics under conditions in which the cargo/importin β concentration ratio is 1:1; total cargo and importin β concentrations were each set to 3 μM. The nuclear concentration of free RanGTP and cytoplasmic concentration of RanBP1 were kept constant (1.23 and 3 μM, respectively) throughout the entire duration of the simulation, which was performed until equilibrium was attained.

The flux rate constants ($k_{in}$ and $k_{out}$) were experimentally determined by in vitro transport assay and are summarized in Table 1. Free EGFP–importin β, as well as importin β bound to cargo (IBB) and RanGTP, shuttles through the NPC in both directions (inward and outward) with similar rate constants (Table 1). The flux rate constants of various cargoes and karyopherins were also obtained and are summarized in Supplemental Figure S2B. The association and dissociation rate constants ($k_{on}$ and $k_{off}$) were obtained by surface plasmon resonance (SPR) using purified recombinant proteins (Supplemental Figure S4; see the Supplemental Experimental Procedure) and are summarized in Table 1. Our model accommodates most of the factors that have been reported to be needed for active nuclear transport; other cofactors, as well as nonspecific competing substrates that abound in the complex cellular milieu, were excluded for ease of computation and analysis.

### Simulating steady-state dynamics of the entire transport cycle

The initial concentrations of cargo and importin β in the cytoplasm were each set at 3 μM, and a RanGTP gradient was formed by maintaining the free RanGTP concentration in the nucleoplasm at a constant value of 1.23 μM throughout the simulation (Riddick and Macara, 2005). The entire system reached steady state before 10 min (Supplemental Figure S5, A and B). The steady-state concentrations and fluxes of each component are summarized in Tables 2 and 3.

The simulation revealed that there are significant influx and efflux of importin β–cargo complex (~0.026 μM/s for the importin β–IBB complex; Table 3), as we observed in FLIP and FRAP analyses (Figures 1 and 3). The influx and efflux of importin β–IBB complex were estimated to be ~29 and ~6 molecules/NPC per second, respectively, given that the volumes of the cytoplasm and nucleoplasm are 5 and 1 pl, respectively, and a single nucleus has ~2700 NPCs (Ribbeck and Gorlich, 2001). The total influx of importin β (free and IBB- and RanGTP-bound forms) was 117 molecules/NPC per second (Table 3), much larger than that of the cargo (29 molecules/NPC per second; Table 3). Indeed, FRAP analysis demonstrated the fast shuttling of EGFP–importin β in vivo (156 molecules/NPC per

| | Reaction/cargo | Kinetic parameter | Parameter value | Assay |
|---|---|---|---|---|
| 1 | Importin β + IBB ⇌ mportin β–IBB | $k_{on}$ | $9.94 \times 10^4$ $M^{-1}$ $s^{-1}$ | SPR |
| | | $k_{off}$ | $1.32 \times 10^{-3}$ $s^{-1}$ | |
| 2 | Importin β – IBB + RanGTP ⇌ Importin β–RanGTP + IBB | $k_{on}$ | $3.89 \times 10^4$ $M^{-1}$ $s^{-1}$ | SPR |
| | | $k_{off}$ | n.d. | |
| 3 | Importin β + RanGTP ⇌ Importin β–RanGTP | $k_{on}$ | $4.44 \times 10^4$ $M^{-1}$ $s^{-1}$ | SPR |
| | | $k_{off}$ | $1.07 \times 10^{-3}$ $s^{-1}$ | |
| 4 | Importin β–RanGTP + RanBP1 ⇌ Importin β + RanGTP–RanBP1 | $k_{on}$ | $3.00 \times 10^5$ $M^{-1}$ $s^{-1}$ | Kuhlmann *et al.* (1997) |
| | | $k_{off}$ | n.d. | |
| 5 | Importin β–$IBB_{cyt}$ ⇌ Importin β–$IBB_{nuc}$ | $k_{in}$ | $6.55 \times 10^{-2}$ $s^{-1}$ | In vitro |
| | | $k_{out}$ | $1.68 \times 10^{-2}$ $s^{-1}$ | Transport |
| 6 | Importin $\beta_{cyt}$ ⇌ Importin $\beta_{nuc}$ | $k_{in}$ | $5.81 \times 10^{-2}$ $s^{-1}$ | In vitro |
| | | $k_{out}$ | $1.07 \times 10^{-2}$ $s^{-1}$ | Transport |
| 7 | Importin β–$RanGTP_{cyt}$ ⇌ Importin β–$GTP_{nuc}$ | $k_{in}$ | $1.78 \times 10^{-2}$ $s^{-1}$ | In vitro |
| | | $k_{out}$ | $2.04 \times 10^{-2}$ $s^{-1}$ | Transport |

n.d., not determined.

TABLE 1: Kinetic parameters of bidirectional nuclear transport determined from SPR and in vitro transport assays.

| | Steady-state concentration (μM) | | | |
|---|---|---|---|---|
| | Importin β–cargo | Free cargo | Free importin β | Importin β–RanGTP |
| Nucleus | 1.54[(a)] | 11.46[(b)] | 0.07[(c)] | 3.81[(d)] |
| Cytoplasm | 0.40[(a')] | 0.004[(b')] | 1.28[(c')] | 0.24[(d')] |

The letters in parentheses correspond to the same letters in the kinetic model (Figure 4). The concentrations of total cargo and importin β were set at 3 μM each.

TABLE 2: Steady-state concentrations of model components.

| Step | | Influx (μM/s) | Efflux (μM/s) |
|---|---|---|---|
| 5 | Importin β–IBB (8 kDa) | 0.026 (29) | 0.026 (6) |
| | Importin β–IBB-mCherry (~40 kDa) | 0.0089 (10) | 0.0089 (2) |
| | Importin β–GST-mCherry-IBB (~70 kDa) | 0.0037 (4) | 0.0037 (1) |
| 6 | Importin β | 0.074 (83) | 0.00071 (0.2) |
| 7 | Importin β–RanGTP | 0.0044 (5) | 0.078 (17) |
| | Total importin β (steps 5 + 6 + 7) | (117) | (23.2) |

Steps 5–7 correspond to the same numbers in the kinetic model (Figure 4) and Table 1. Number of molecules/NPC per second is given in parentheses. Details of its estimation are presented in the text (*Results*).

TABLE 3: Steady-state flux of karyopherins and cargoes in the kinetic model.

second at an EGFP–importin β concentration of 1 μM; Table 4 and Supplemental Figure S3A).

At steady state, the nuclear/cytoplasmic (nuc/cyt) ratio of total cargo (free and importin β–bound forms) was ~32, whereas that of total importin β (free and cargo- and RanGTP-bound forms) was 2.8. The nuc/cyt ratio of cargo was not affected by influx and efflux rate constants of importin β–cargo complex ($k_{in}$[impβ-cargo] and $k_{out}$[impβ-cargo], respectively); they only affect the time required to reach equilibrium (Supplemental Figure S5C). In contrast, the steady-state cargo fluxes largely depend on $k_{in}$ and $k_{out}$ values of the importin β–cargo complex (Table 3) and therefore on the cargo size (Figure 3). Cargoes with ~40 and ~70 kDa showed steady-state influxes of ~10 and 4 molecules/NPC per second, respectively. These values are in good agreement with flux of 1–10 molecules/NPC per second determined in the FLIP and FRAP analyses (Figures 1 and 3 and Table 4).

Further confirmation of the fidelity of our model was obtained by simulating the effect of RanGTP on the steady-state flux. The nuclear concentration of RanGTP was titrated from 0.01 to 10 μM in the model. As the RanGTP concentration increased, the steady-state nuclear accumulation of the cargo also accelerated (Supplemental Figure S5D), and this was confirmed experimentally (Supplemental Figure S5E).

Collectively, all of these results demonstrate that our kinetic model can explain the in vivo steady-state dynamics of karyopherin-dependent transport cycle.

### How the cargo/karyopherin ratio affects the steady-state dynamics of transport

Considering that a single karyopherin carries multiple and different cargoes, it is important to simulate how the steady-state cargo distribution and flux are affected by different cargo/karyopherin (cargo/kap) ratios. The foregoing kinetic simulation was performed at a fixed amount of importin β (3 μM) and various amounts of initial cytoplasmic cargo (0.5–50 μM). As the cargo/kap concentration ratio increased, accumulation of the cargo in the nucleus (nuc/cyt ratio) increased (Figure 5A). However, in the presence of excess cargo (cargo/kap concentration ratio >1), there was no significant change in the steady-state concentration (Table 5) and flux of free importin β (Figure 5B) and importin β–cargo complex (Figure 5C). Conversely, in the presence of excess karyopherin (cargo/kap concentration ratio <1), fluxes of importin β-cargo increased in a cargo/kap ratio–dependent manner, indicating that karyopherin availability might be a rate-limiting factor in the transport process.

### Rate-limiting step in the import process

We then compared the steady-state fluxes with the binding/unbinding reaction rates ($v_{on}$ and $v_{off}$, respectively) to elucidate the rate-limiting step of cargo transport. We compared three steps of the import process: 1) importin β binding to the cargo (Figure 4, step 1 in the cytoplasm), 2) influx of importin β–cargo through the NPC (step 5), and 3) RanGTP-dependent cargo release from importin β (step 2). At all cargo/kap ratios simulated, the rate of importin β–cargo binding ($5.22 \times 10^{-4}$ μM/s) is much slower than the influx rate ($2.59 \times 10^{-2}$ μM/s), as well as the cargo-release rate ($7.38 \times 10^{-2}$ μM/s; Figure 5D), demonstrating that importin β–cargo binding in the cytoplasm is the rate-limiting step in the import process.

This result also elucidates the fate of the importin β–cargo complex in the nucleus; whether it releases the cargo (step 2, on), or travels back to the cytoplasm (step 5, out). Figure 5D indicates that at steady state, the rates of these two steps are comparable ($7.38 \times 10^{-2}$ μM/s for cargo release and $2.59 \times 10^{-2}$ μM/s for efflux), although the cargo-release step slightly dominates the efflux. These

| Cargo | Size (kDa) | $k_{in}$ ($\times 10^{-3}$ $s^{-1}$) | $k_{out}$ ($\times 10^{-3}$ $s^{-1}$) | Influx (μM/s) | Efflux (μM/s) |
|---|---|---|---|---|---|
| No cargo (free importin β) | 0 | 140 | 3.5 | 0.1400 (156) | 0.0035 (3.9) |
| EGFP-eIF1A | ~50 | 2.1 | 1.1 | 0.0021 (2.3) | 0.0011 (1.3) |
| EGFP-rpL23A | ~50 | | 1.0 | n.d. | 0.0010 (1.1) |
| EGFP-Snail | ~60 | 9.0 | 3.3 | 0.0090 (10) | 0.0033 (3.7) |
| cNLS-EGFP-eIF4A1 | ~73 | 1.6 | | 0.0016 (1.8) | n.d. |
| EGFPx3-cNLS | ~100 | 1.0 | 1.4 | 0.0010 (1.1) | 0.0014 (1.6) |

A steady-state concentration of 1 μM was used for the flux calculation (details in the Supplemental Experimental Procedure). Number of molecules/NPC per second is given in parentheses. n.d., not determined.

TABLE 4: Steady-state flux of cargoes in vivo.

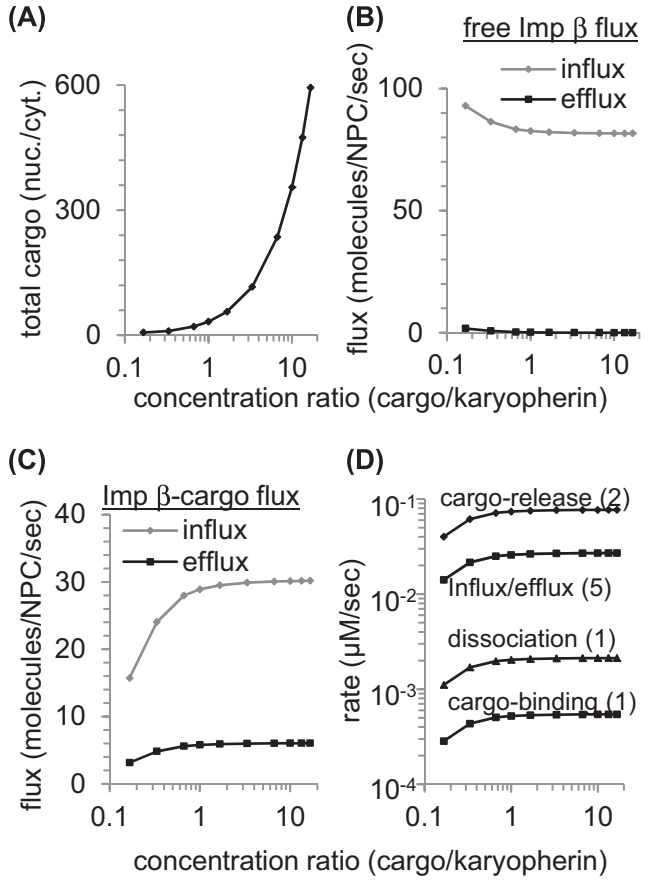


FIGURE 5: Kinetic simulation of conditions that may affect steady-state cargo flux/distribution. (A–D) Cargo concentration was varied from 0.5 to 50 μM and karyopherin concentration kept constant at 3 μM. Steady-state concentration ratio of total cargo (free + bound) in the nucleus and the cytoplasm (A), free importin β influx/efflux (B), and importin β-cargo influx/efflux (C) were obtained and are plotted against cargo/karyopherin (cargo/kap) concentration ratios. (D) Nuclear steady-state concentrations of importin β-cargo complex were integrated with $k_{off}$[importin β-cargo], $k_{on}$[importin β-RanGTP], and $k_{out}$[importin β-cargo] to derive the different rates of spontaneous dissociation (Figure 4, step 1), RanGTP-dependent cargo release (step 2), and efflux (step 5). Similarly, the cytoplasmic steady-state concentrations of free importin β and free cargo were combined with the $k_{on}$ of step 1 to determine the rate of formation ($v_{on}$) of importin β–cargo complex. These fluxes, together with the influx rates (step 5) of importin β–cargo, are plotted for the different cargo/kap concentration ratios as shown.

results again demonstrate that a significant portion of the imported cargo is shuttling across the NPC.

## DISCUSSION

A number of in vitro transport studies established the karyopherin-dependent transport process of cargo proteins through the NPC: importins, with or without the aid of an adaptor molecule such as importin α, bind their cognate cargoes in the cytoplasm, where a low concentration of RanGTP exists, dock at NPCs, and interact with nucleoporins as they translocate through the NPCs; finally, upon their encounter with a higher concentration of RanGTP on the nucleocytoplasmic face of the NPC, the cargo dissociates (Ribbeck *et al.*, 1998; Fahrenkrog and Aebi, 2003). These in vitro studies are indispensable, as they provide kinetic parameters of the transport steps involving different types of cargo and transport receptors, and also reveal how the parameters are affected by factors such as concentration, molecular size, and modifications. Equally important are in vivo analyses of transport events, using time-lapse fluorescence observation, to provide the intracellular dynamics of each component (cargo or transport receptors). However, the detailed molecular state of the labeled protein (whether it is free, bound with the cargo, or bound with RanGTP) is not clear. Therefore, in this study, we combined in vivo and in vitro experimental systems to explain the detailed dynamics of nuclear transport components in a living cell. We measured actual flux rates and determined how thermodynamic considerations drive cargo redistribution between the nucleus and the cytoplasm.

### Intracellular dynamics of karyopherin–cargo complexes

The in vivo FLIP analysis of fluorescently labeled cargo showed that the ~100-kDa EGFPx3-cNLS was exported from the nucleus in a CRM1-independent manner when the cytoplasm was continuously photobleached (Figure 1 and Supplemental Figure S1C). This is a strong indication that importin β1 serves as an export mediator for the ~100-kDa cNLS-cargo. A similar inference was drawn by Kopito and Elbaum (2007) in an in vitro system in which they deployed FRAP to bleach reconstituted nuclei that had accumulated GFP-nucleoplasmin in the presence of importin α/β. They inferred that the fluorescence recovery in the nuclei was evidence of reversibility of nuclear transport, positing that an influx of fluorescent cargo could only have been at the instance of the efflux of bleached molecules. Our approach provides in vivo evidence for the emerging concept of nuclear transport reversibility.

Our results also strongly indicate that bidirectional cargo translocation is not a peculiar feature of importin β1 but seems to be a general feature of karyopherins, considering that EGFP-Snail (~60 kDa), EGFP-eIF1A (~50 kDa), and EGFP-rpL23A (~50 kDa)—the respective cargoes for importins β1, 13, and 5—exhibit similar nuclear efflux tendencies during FLIP analysis (Figure 1). These findings agree with one of the earliest studies to link nuclear import of nucleolin and its shuttling after transient transfection and microinjection into HeLa cells (Schmidt-Zachmann *et al.*, 1993). Our results are also consistent with subsequent microinjection studies that proved that proteins such as pyruvate kinase and β-galactosidase, which are exclusively cytosolic, could shuttle bidirectionally when an NLS (either the classical or M9 sequence) is grafted onto them (Guiochon-Mantel *et al.*, 1994; Michael *et al.*, 1995). Indeed, our observation of a bidirectional karyopherin–cargo flux across the nuclear envelope might explain a very early puzzle that led Michael *et al.* (1995) to

| | Steady-state concentration (μM) at given level of titration | | | | | | | |
|---|---|---|---|---|---|---|---|---|
| | 0.5 μM | 1 μM | 2 μM | 3 μM | 5 μM | 10 μM | 20 μM | 50 μM |
| Nucleus | 0.84 | 1.28 | 1.50 | 1.54 | 1.57 | 1.60 | 1.61 | 1.68 |
| Cytoplasm | 0.22 | 0.33 | 0.38 | 0.40 | 0.40 | 0.41 | 0.41 | 1.43 |

Total cargo concentration was titrated from 0.5 to 50 μM, and the concentration of total importin β was fixed at 3 μM.

TABLE 5: Steady-state concentrations of importin β-cargo upon titration of cargo concentration in the kinetic model.

conclude that the M9 sequence of hnRNPA1 serves as both an NLS and an NES. In addition, our in vivo experiments confirm an earlier in vitro observation that, in the absence of a RanGTP gradient, importin 13 was still able to appreciably export eIF1A from permeabilized HeLa nuclei (Mingot *et al.*, 2001; Grunwald *et al.*, 2013). Our in vitro experiments, using purified components and semipermeabilized HeLa cells, give direct proof that NLS cargoes, complexed with importins, do shuttle the NPCs in both directions (Figure 2).

### Which interaction is rate limiting: karyopherin–nucleoporin or karyopherin–cargo?

At 1 μM steady-state nuclear concentration of karyopherin–cargo complex, the different cargoes investigated had flux rates of 1–10 molecules/NPC per second (Table 4). The computed values largely agree with our kinetic predictions, as well as with values obtained by other researchers using cell extracts and microinjection approaches (Keminer *et al.*, 1999; Nemergut and Macara, 2000). However, the values are far lower than the maximum flux of ~1000 molecules/NPC per second calculated in an earlier in vitro study of non–steady-state kinetics involving higher initial concentrations of cargoes (Ribbeck and Gorlich, 2001).

The low cargo flux in vivo raises the question of which step might be rate limiting in the entire transport cycle. A comparison of the rate of karyopherin–cargo complex formation in the cytosol (Figure 4, step 1) with the influx rate of the complex into the nucleus (step 5) revealed that the latter reaction step is faster than the former at all cargo/kap concentration ratios simulated (Figure 5D). This suggests that importin β–cargo interaction, rather than cargo translocation, is much slower in the steady-state transport. Collectively, these findings are in consonance with previous reports suggesting that the determinants of nuclear transport are receptor–cargo affinity and the ease of locating specific cargoes within the complex cellular milieu of numerous nonspecific substrates (Smith *et al.*, 2002; Timney *et al.*, 2006; Kim and Elbaum, 2013).

The finding that nuclear pore permeability is not rate limiting does not reduce its significance as a key factor in the transport process. In fact, it has been argued that free karyopherins constantly occupy the NPCs to exclude interaction of nonspecific molecules, thereby enhancing the selectivity of the pores (Zilman *et al.*, 2007). This view is supported by our kinetic simulations, which revealed that, at a cargo/kap ratio of 1:1, free importin β had a high steady-state influx of ~83 molecules/NPC per second, compared with either importin β-RanGTP and importin β-cargo rates, which were 20 and 3 times lower, respectively (Table 3). Our study shows that bidirectional flux is not restricted to free karyopherins alone but also includes karyopherin–cargo complexes.

Bidirectionality could also be a cellular mechanism to optimally conserve energy, given that the recycling step in a unidirectional model would be energetically costly. Another significance of bidirectional flux is that it could complement the cell's ability to ensure proper distribution of cargoes in both the nucleus and the cytoplasm. This is conceivable, considering that previous studies reported that cells are equipped with many strategies to export proteins (such as initiation factors) that are otherwise cytosolic but are still capable of reentering the nucleus by diffusion or active transport if they possess cryptic NLSs (Bohnsack *et al.*, 2002).

### RanGTP gradient is not essential for bidirectional cargo transport

Thus far, our data show that karyopherins lack inherent directionality and there is constant bidirectional flux of molecules across the NPCs, as guaranteed by the laws of thermodynamics for a system at steady state. Cargo properties such as size and hydrophobicity—not RanGTP concentration—are the key factors in determining the influx and efflux rates of the karyopherin–cargo complex (Figures 3 and 5D). It seems that the RanGTP gradient mainly functions to ensure that steady-state concentrations of the cargo are attained in the appropriate destination. This is most certainly correct, considering the established fact that incubation of digitonin-permeabilized cells with karyopherins and cargoes, in the absence of Ran, leads to nuclear accumulation of cargo to the same level as the extranuclear space (Supplemental Figure S6). These lines of argument concur with earlier findings that thermodynamic factors have a significant influence on nuclear transport (Kopito and Elbaum, 2009).

These findings agree with earlier and more recent works that suggest that there is practically no requirement for Ran in determining the direction of transport or flux rates of relatively small cargoes (~50–120 kDa; Lyman *et al.*, 2002; Lowe *et al.*, 2015). However, RanGTP might be needed for the translocation of very large cargoes (~200 kDa and above). In the absence of RanGTP, a portion of the pool of importin β binds stably to Nup153 on the nucleoplasmic face of the NPC, thereby reducing the number of free karyopherin molecules needed for cargo accumulation. Addition of RanGTP reduces the interaction of importin β with Nup153 such that the pool of available karyopherin is increased to effect dramatic accumulation of cargo. Such Ran-dependent karyopherin–Nup interactions will be considered in future modeling analysis.

### Conclusion

Besides contributing to NPC selectivity, bidirectional flux of free and bound karyopherins may also be a sort of regulatory mechanism that the cell uses to continuously scrutinize the quality and optimal concentration of intracellular transportable components, whereas it uses other factors, such as the RanGTP gradient, to drive cargo accumulation and net transport in the appropriate compartment.

## MATERIALS AND METHODS

### DNA constructs and purification of proteins

Mouse importin β (GST tagged), human RanGTP, and RanGDP were prepared as described in a previous study (Inamoto *et al.*, 1995). The proteins were expressed as GST fusion proteins and subjected to specific protease digestion (PreScission; GE Healthcare, Little Chalfont, United Kingdom) if necessary. The cDNA fragment encoding the importin β–binding domain of rat importin α (IBB, amino acids 1–66) was amplified by PCR and cloned into a pET29 vector (Novagen, Darmstadt, Germany). The protein was expressed in *Escherichia coli* and purified by ion-exchange chromatography (Hi-Trap SP; GE Healthcare) and finally by gel filtration chromatography (Superdex 75, GE healthcare). The cDNA encoding human CRM1 was a kind gift from M. Ohno (Kyoto University, Kyoto. Japan), and expression vectors for importin β, Snail, and SREBP2 were provided by Y. Yoneda (Osaka University, Osaka, Japan). For the expression and purification of recombinant hCRM1, cDNA encoding human CRM1 was subcloned into vector pQE60 (Qiagen, Valencia, CA) so that a hexahistidine tag was attached at the carboxy terminus. To construct GFP-fusion hCRM1, cDNA encoding GFP was amplified and inserted after the CRM1-coding region. The plasmid was introduced into a *E. coli* strain TG1 (Zymo Research, Irvine, CA), and the expression of fusion protein was induced by 0.5 mM isopropyl-β-D-thiogalactoside at 21°C for 6 h. The cell lysate was subjected to ammonium sulfate precipitation and histidine-Trap affinity chromatography using the FPLC system (GE Healthcare). The peak fraction was further subjected to either Mono-Q ion-exchange chromatography and subsequent

Superdex200 size-exclusion chromatography (for GFP-hCRM1) or HiTrap Q ion-exchange chromatography (for hCRM1; all from GE Healthcare). cDNA encoding human eIF1A and rpL23A were purchased from the Kazusa DNA Research Institute (Kisarazu, Japan) and inserted in-frame into a pEGFP-C1 vector (Invitrogen, Carlsbad, CA) to form the EGFP-eIF1A and EGFP-rpL23A DNA constructs used for transfection of HeLa cells.

### FLIP and FRAP analyses

Three tandem EGFPs fused with the NLS of SV40 large T-antigen (EGFPx3-cNLS), EGFP-Snail, EGFP-SREBP2, EGFP-eIF1A, EGFP-rpL23A, or eIF4A1 fused with SV40 NLS was expressed in HeLa cells. Photobleaching, observation, and image acquisition were performed by confocal laser scanning microscopy (Zeiss-META and Olympus FV 1200). The microscope sample chamber was maintained at 37°C with a constant stream of 5% $CO_2$ during live-cell imaging. For the time-lapse imaging of FRAP and FLIP, three images were acquired before commencement of bleaching, and all post-bleaching images were acquired with 1% laser intensity to reduce loss of fluorescence intensity. For the FLIP experiments, a defined area of the cytoplasm was alternately irradiated by laser at the maximum output for 2 s, and images were captured for 15 s between rounds of irradiation for 30 min. Images were analyzed by subtracting background signals and expressing nuclear fluorescence intensity relative to the prebleach intensity. For the FRAP experiments, the entire nucleus was photobleached at maximum output for 72 ms (EGFP-importin β) and 5 s (EGFP-labeled cargoes). Nuclear fluorescence recovery images were captured every 63 ms for 20 s (EGFP-importin β) and every 3 s for 20 min (EGFP-labeled cargoes). Fluorescence recovery was expressed as fluorescence intensity relative to prebleach intensity.

### In vitro nuclear transport assay

HeLa cells were washed with transport buffer (20 mM 4-(2-hydroxyethyl)-1-piperazineethanesulfonic acid [HEPES]-KOH, pH 7.3, 110 mM $CH_3COOK$, 2 mM $(CH_3COO)_2Mg$, 5 mM $CH_3COONa$, 0.5 mM ethylene glycol tetraacetic acid [EGTA], and 1 mM dithiothreitol) and incubated with 40 µg/ml digitonin at 0°C for 5 min. The cells were washed twice with transport buffer and incubated at 37°C for 15 min. The time-lapse observation by fluorescence microscopy (Zeiss-META) was started just after the addition of purified EGFP-fused karyopherin (1–5 µM). We added 10 µg/ml Alexa 568–labeled immunoglobulin G or 1 µM rhodamine-linked 70-kDa Dextran to the sample to verify the integrity of the nuclear envelope.

### Kinetic analysis of protein–protein interaction by surface plasmon resonance

The sensor chip for SPR (Moritex, Japan) was first treated with 4,4′-dithio dibutyric aid (DDA) to form a self-assembled monolayer on the chip surface. Streptavidin was covalently cross-linked to DDA by 1-ethyl-3-[3-dimethylaminopropyl]carbdiimide and N-hydroxysuccinimide. Biotinylated protein was then fixed on the chip surface by injection. Running buffer with and without analyte protein was injected in sensing and reference channels, respectively. The composition of the running buffer is 20 mM HEPES-KOH (pH 7.3), 110 mM $CH_3COOK$, 2 mM $(CH_3COO)_2Mg$, 5 mM $CH_3COONa$, and 0.5 mM EGTA. To prepare biotinylated protein, the GST-fused target protein carrying biotin-binding peptide sequence (GLNDIFEAQKIEWHE) at the carboxy terminus was expressed in an *E. coli* strain expressing biotin ligase (AVB101; Avidity) in the presence of 5 µM D-biotin, purified by glutathione–Sepharose beads (GE Healthcare), and separated from GST moiety by site-specific protease cleavage (PreCission).

### Image analysis and kinetic analysis

All of the microscopic image analyses were performed by MetaMorph software (Molecular Imaging). Curve fitting and other kinetic analyses of obtained data were performed by Origin software (Light Stone). All molecular simulations were done by CellDesigner 4.4.

## ACKNOWLEDGMENTS

This work was supported by a Funding Program for Next Generation World-leading Researchers (S.H.Y.), a Grant-in-Aid for Scientific Research (B) (S.H.Y.), a Grant-in-Aid for Young Scientists (A) (S.H.Y.), and a Grant-in-Aid for Young Scientists (B) (M.K.) from the Japan Society for the Promotion of Science, a Grant-in-Aid for Scientific Research on Innovative Areas (M.K.) from the Ministry of Education, Culture, Sports, Science and Technology, Japan, and a Cross-Disciplinary Research Promotion Project from the Institute for Integrated Cell-Material Sciences, Kyoto University, Japan (M.K.).

## REFERENCES

Ben-Efraim I, Gerace L (2001). Gradient of increasing affinity of importin b for nucleoporins along the pathway of nuclear import. J Cell Biol 152, 411–417.

Bischoff FR, Gorlich D (1997). RanBP1 is crucial for the release of RanGTP from importin b-related nuclear transport factors. FEBS Lett 419, 249–254.

Bohnsack MT, Regener K, Schwappach B, Saffrich R, Paraskeva E, Hartmann E, Gorlich D (2002). Exp5 exports eEF1A via tRNA from nuclei and synergizes with other transport pathways to confine translation to the cytoplasm. EMBO J 21, 6205–6215.

Cansizoglu AE, Lee BJ, Zhang ZC, Fontoura BM, Chook YM (2007). Structure-based design of a pathway-specific nuclear import inhibitor. Nat Struct Mol Biol 14, 452–454.

Chook YM, Blobel G (1999). Structure of the nuclear transport complex karyopherin-b2–Ran.GppNHp. Nature 399, 230–237.

Cingolani G, Bednenko J, Gillespie MT, Gerace L (2002). Molecular basis for the recognition of a nonclassical nuclear localization signal by importin Beta. Mol Cell 10, 1345–1353.

Cingolani G, Petosa C, Weis K, Muller CW (1999). Structure of importin-beta bound to the IBB domain of importin-alpha. Nature 399, 221–229.

Fahrenkrog B, Aebi U (2003). The nuclear pore complex: nucleocytoplasmic transport and beyond. Nat Rev Mol Cell Biol 4, 757–766.

Fahrenkrog B, Stoffler D, Aebi U (2001). Nuclear pore complex architecture and functional dynamics. Cur Top Microbiol Immunol 259, 95–117.

Frey S, Gorlich D (2007). A saturated FG-repeat hydrogel can reproduce the permeability properties of nuclear pore complexes. Cell 130, 512–523.

Frey S, Richter RP, Gorlich D (2006). FG-rich repeats of nuclear pore proteins form a three-dimensional meshwork with hydrogel-like properties. Science 314, 815–817.

Gorlich D, Kutay U (1999). Transport between the cell nucleus and the cytoplasm. Annu Rev Cell Dev Biol 15, 607–660.

Gorlich D, Pante N, Kutay U, Aebi U, Bischoff FR (1996). Identification of different roles for RanGDP and RanGTP in nuclear protein import. EMBO J 15, 5584–5594.

Gorlich D, Seewald MJ, Ribbeck K (2003). Characterization of Ran-driven cargo transport and the RanGTPase system by kinetic measurements and computer simulation. EMBO J 22, 1088–1100.

Grunwald M, Lazzaretti D, Bono F (2013). Structural basis for the nuclear export activity of importin 13. EMBO J 32, 899–913.

Guiochon-Mantel A, Delabre K, Lescop P, Milgrom E (1994). Nuclear localization signals also mediate the outward movement of proteins from the nucleus. Proc Natl Acad Sci USA 91, 7179–7183.

Hutten S, Flotho A, Melchior F, Kehlenbach RH (2008). The Nup358-RanGAP complex is required for efficient importin a/b-dependent nuclear import. Mol Biol Cell 19, 2300–2310.

Inamoto N, Shimamoto T, Kose S, Takao T, Tachibana T, Matsubae M, Sekimoto T, Shimonishi Y, Yoneda Y (1995). The nuclear pore-targeting complex binds to nuclear pores after association with a karyophile. FEBS Lett 368, 415–419.

Jang BC, Najar UM, Paik JH, Claffey K, Yoshida M, Hla T (2003). Leptomycin B, an inhibitor of the nuclear export receptor CRM1, inhibits COX-2 expression. J Biol Chem 275, 2773–2776.
Keminer O, Siebrasse JP, Zerf K, Peters R (1999). Optical recording of signal-mediated protein transport through single pore complexes. Proc Natl Acad Sci USA 96, 11842–11847.
Kim S, Elbaum M (2013). A simple kinetic model with explicit predictions for nuclear transport. Biophys J 105, 565–569.
Kopito RB, Elbaum M (2007). Reversibility of nucleocytoplasmic transport. Proc Natl Acad Sci USA 104, 12743–12748.
Kopito RB, Elbaum M (2009). Nucleocytoplasmic transport: a thermodynamic mechanism. HFSP J 3, 130–141.
Kudo N, Wolff B, Sekimoto T, Schreiner EP, Yoneda Y, Yanagida M, Horinouchi S, Yoshida M (1998). Leptomycin B inhibition of signal-mediated nuclear export by direct binding of CRM1. Exp Cell Res 242, 540–547.
Kuhlmann J, Macara I, Wittinghofer A (1997). Dynamic and equilibrium studies on the interaction of Ran with its effector, RanBP1. Biochemistry 36, 12027–12035.
Kumeta M, Yamaguchi H, Yoshimura SH, Takeyasu K (2012). Karyopherin-independent spontaneous transport of amphiphilic proteins through the nuclear pore. J Cell Sci 125, 4979–4984.
Kumeta M, Yoshimura SH, Harata M, Takeyasu K (2010). Molecular mechanisms underlying nucleocytoplasmic shuttling of actinin-4. J Cell Sci 123, 1020–1030.
Lee SJ, Sekimoto T, Yamashita E, Nagoshi E, Nakagawa A, Imamoto N, Yoshimura M, Sakai H, Chong KT, Tsukihara T, Yoneda Y (2003). The structure of importin b bound to SREBP-2: nuclear import of a transcription factor. Science 302, 1571–1575.
Lim RYH, Huang NP, Koser J, Deng J, Lau KHA, Schwarz-Herion K, Fahrenkrog B, Aebi U (2006). Flexible phenylalanine-glycine nucleoporins as entropic barriers to nucleocytoplasmic transport. Proc Natl Acad Sci USA 103, 9512–9517.
Lowe AR, Tang JH, Yassif J, Graf M, Huang WYC, Groves JT, Weis K, Liphardt JT (2015). Importin b modulates the permeability of the nuclear pore complex in a Ran-dependent manner. Elife 4, e04052.
Lyman SK, Guan T, Bednenko J, Wodrich H, Gerace L (2002). Influence of cargo size on Ran and energy requirements for nuclear protein import. J Cell Biol 159, 55–67.
Michael WM, Choi M, Dreyfuss G (1995). A nuclear export signal in hnRNPA1: a signal-mediated, temperature-dependent nuclear protein export pathway. Cell 83, 415–422.
Mingot J, Kosta S, Kraft R, Hartmann E, Gorlich D (2001). Importin 13: a novel mediator of nuclear import and export. EMBO J 20, 3685–3694.
Miyamoto Y, Saiwaki T, Yamashita J, Yasuda Y, Kotera I, Shibata S, Shigeta M, Hiraoka Y, Haraguchi T, Yoneda Y (2004). Cellular stresses induce the nuclear accumulation of importin a and cause a conventional nuclear import block. J Cell Biol 165, 617–623.
Nemergut ME, Macara IG (2000). Nuclear import of Ran Exchange Factor, RCC1, is mediated by at least two distinct mechanisms. J Cell Biol 149, 835–849.
Ohno M, Fornerod M, Mattaj IW (1998). Nucleocytoplasmic transport: the last 200 nanometers. Cell 92, 327–336.
Paine PL, Moore LC, Horowitz SB (1975). Nuclear envelope permeability. Nature 254, 109–114.
Pante N, Kann M (2002). Nuclear pore complex is able to transport macromolecules with diameters of ~39 nm. Mol Biol Cell 13, 425–434.
Patel SS, Belmont BJ, Sante JM, Rexach MF (2007). Natively unfolded nucleoporins gate protein diffusion across the nuclear pore complex. Cell 129, 83–96.
Peters R (2009). Translocation through the nuclear pores: kaps pave the way. Bioessays 31, 466–477.
Ribbeck K, Gorlich D (2001). Kinetic analysis of translocation through nuclear pore complexes. EMBO J 20, 1320–1330.
Ribbeck K, Gorlich D (2002). The permeability of the nuclear pore complexes appears to operate via hydrophobic exclusion. EMBO J 21, 2664–2671.
Ribbeck K, Lipowsky G, Kent HM, Stewart M, Gorlich D (1998). NTF2 mediates nuclear import of Ran. EMBO J 17, 6587–6598.
Riddick G, Macara IG (2005). A system analysis of importin-a-b-mediated nuclear protein import. J Cell Biol 168, 1027–1038.
Rout MP, Aitchison JD (2001). The nuclear pore complex as a transport machine. J Biol Chem 276, 16593–16596.
Rout MP, Aitchison JD, Suprapto A, Hjertaas K, Zhao YM, Chait BT (2000). The yeast nuclear pore complex: composition, architecture and transport mechanism. J Cell Biol 148, 625–651.
Schmidt-Zachmann MS, Dargemont C, Kuhn LC, Nigg EA (1993). Nuclear export of proteins: the role of nuclear retention. Cell 74, 493–504.
Shah S, Forbes DJ (1998). Separate nuclear import pathways converge on the nucleoporin 153 and can be dissected with dominant-negative inhibitors. Curr Biol 8, 1376–1386.
Smith AE, Slepchenko BM, Schaff JC, Loew LM, Macara IG (2002). Systems analysis of Ran transport. Science 295, 488–491.
Strom A, Weis K (2001). Importin-b-like nuclear transport receptors. Genome Biol 2, 3008.1.
Tetenbaum-Novatt J, Hough LE, Mironska R, McKenney AS, Rout MP (2012). Nucleocytoplasmic transport: a role for nonspecific competition in karyopherin-nucleoporin interactions. Mol Cell Proteomics 11, 31–46.
Timney B, Tetenbaum-Novatt J, Agate D, Williams R, Zhang W, Chait BT, Rout MP (2006). Simple kinetic relationships and nonspecific competition govern nuclear import rates *in vivo*. J Cell Biol 175, 579–593.
Van der Watt PJ, Maske CP, Hendricks DT, Parker MI, Denny L, Govender D, Birrer MJ, Leaner VD (2009). The karyopherin proteins, Crm1 and karyopherin beta1, are overexpressed in cervical cancer and are critical for cancer cell survival and proliferation. Int J Cancer 124, 1829–1840.
Vasu SK, Forbes DJ (2001). Nuclear pores and nuclear assembly. Curr Opin Cell Biol 13, 363–375.
Wente SR, Rout MP (2010). The nuclear pore complex and nuclear transport. Cold Spring Harb Perspect Biol 2, a000562.
Yang W, Musser SM (2006). Nuclear import time and transport efficiency depend on importin beta concentration. J Cell Biol 174, 951–961.
Yaseen NR, Blobel G (1997). Cloning and characterization of human karyopherin b3. Proc Natl Acad Sci USA 94, 4451–4456.
Yoshimura SH, Kumeta M, Takeyasu K (2014). Structural mechanism of nuclear transport mediated by importin b and flexible amphiphilic proteins. Structure 22, 1699–1710.
Zilman A, Di Talia S, Chait BT, Rout MP, Magnasco MO (2007). Efficiency, selectivity and robustness of nucleocytoplasmic transport. PLoS Comput Biol 3, e125.